Source Analysis of Event-related Cortical Activity during Visuo-spatial Attention

Francesco Di Russo[1,2,3], Antigona Martínez[1,4] and Steven A. Hillyard[1]

[1]Department of Neurosciences, University of California San Diego, La Jolla, CA, USA, [2]Fondazione Santa Lucia, IRCCS, Rome, [3]Istituto Universitario di Scienze Motorie, IUSM, Rome, Italy and [4]Nathan S. Kline Institute for Psychiatric Research, Program in Cognitive Neuroscience and Schizophrenia, New York, USA

Recordings of event-related potentials (ERPs) were combined with structural and functional magnetic resonance imaging (fMRI) to study the spatio-temporal patterns of cortical activity that underlie visual–spatial attention. Small checkerboard stimuli were flashed in random order to the four quadrants of the visual field at a rapid rate while subjects attended to stimuli in one quadrant at a time. Attended stimuli elicited enhanced ERP components in the latency range 80–200 ms that were co-localized with fMRI activations in multiple extrastriate cortical regions. The earliest ERP component (C1 at 50–90 ms) was unaffected by attention and was localized by dipole modeling to calcarine cortex. A longer latency deflection in the 150–225 ms range that was accounted for by this same calcarine source, however, did show consistent modulation with attention. This late attention effect, like the C1, inverted in polarity for upper versus lower field stimuli, consistent with a neural generator in primary visual cortex (area V1). These results provide support to current hypotheses that spatial attention in humans is associated with delayed feedback to area V1 from higher extrastriate areas that may have the function of improving the salience of stimuli at attended locations.

Introduction

The human visual system can focus attention in a spatially selective manner in order to facilitate the perception of stimuli within a restricted zone of the visual field (LaBerge, 1995; Wright, 1998). Studies in both animals and humans have sought to specify the levels of visual-cortical processing at which incoming sensory information is modulated by spatial attention. Neurophysiological recordings from monkeys have shown that neural activity elicited by attended-location stimuli is enhanced in multiple regions of the extrastriate visual cortex including retinotopic areas V2, V3a and V4 as well as in higher areas belonging to both the dorsal and ventral processing streams (Maunsell and McAdams, 2000; Reynolds and Desimone, 2001). Recent experiments in monkeys have also found that neural activity in primary visual cortex may be modulated by attention under certain conditions, in particular when several competing stimuli are present (Motter, 1993; Roelfsema *et al.*, 1998; Vidyasagar, 1998; Ito and Gilbert, 1999). Enhanced neural responses in area V1 were typically found to occur at fairly long latencies (80–100 ms or more), well beyond the initial peak of the sensory-evoked response, suggesting that the attentional modulations were carried out via delayed feedback influences from higher visual areas (Vidyasagar, 1999). In support of such a feedback mechanism, Mehta and collaborators (Mehta *et al.*, 2000a,b) found that evoked activity in higher tier visual areas such as V4 were modulated by attention at shorter latencies than was activity in area V1.

The participation of primary visual cortex in spatial attention is further evidenced by recent neuroimaging studies in humans (Tootell *et al.*, 1998; Brefczynski and DeYoe, 1999; Ghandhi *et al.*, 1999; Martínez *et al.*, 1999; Somers *et al.*, 1999). Using fMRI, these studies found that paying attention to a stimulus resulted in increased neural activity in restricted zones of area V1 (and of higher extrastriate areas as well) that corresponded to the retinotopic projection of the attended location. Considering the low temporal resolution of fMRI, however, it was difficult to determine whether these attention-related increases in neural activity in V1 reflected a modulation of early sensory-evoked activity in V1, a delayed modulation of V1 activity produced by feedback from higher areas, or a sustained increase or bias in ongoing neural activity associated with the spatial focusing of attention (Luck *et al.*, 1997; Kastner *et al.*, 1999; Ress *et al.*, 2000).

Information about the time course of attentional selection processes in striate and extrastriate areas has come from recordings of event-related potentials (ERPs) and event-related magnetic fields (ERFs) from the human brain. Stimuli at attended locations have been found to elicit enlarged P1 (latency 80–130 ms) and N1 (150–200 ms) components in the ERP over the posterior scalp, which have been localized through dipole source modeling and co-registration with blood-flow neuroimaging to specific zones of extrastriate visual cortex (Heinze *et al.*, 1994; Clark and Hillyard, 1996; Woldorff *et al.*, 1997; Wijers *et al.*, 1997; Martínez *et al.*, 1999; Mangun *et al.*, 2001). These amplitude modulations support the view that spatial attention exerts a selective gain control or amplification of attended inputs in extrastriate cortex during the interval 80–200 ms following stimulus onset (Hillyard *et al.*, 1998).

In the aforementioned ERP studies it was further observed that the earlier C1 component (onset latency 50–60 ms) was not modified by spatial attention. There is a good deal of evidence that the C1 represents the initial evoked response in primary visual cortex based on its short onset latency, its retinotopic polarity inversion in scalp recordings, and the localization of its neural generators to the calcarine cortex in close proximity to area V1 (Clark *et al.*, 1995; Mangun, 1995; Martínez *et al.*, 1999; Di Russo *et al.*, 2001b). Taken together, these ERP results suggest that the initial geniculostriate evoked response in area V1 is not modulated by spatial attention and that the earliest attentional influences are upon visual processing in extrastriate areas starting at ~70–80 ms.

A recent study by Martínez and colleagues (Martínez *et al.*, 1999) carried out ERP recordings and fMRI (on separate days) as subjects attended to a rapid sequence of stimuli presented to one visual field while ignoring a comparable sequence to the opposite field. As in previous studies, the C1 amplitude was found to be unaffected by attention, but its dipolar source was co-localized with a zone of attention-related neural activity in area V1 as shown by fMRI. To account for this apparent discrepancy, dipole modeling of the ERP attention effects revealed a delayed response at 150–250 ms attributed to the same calcarine source as the C1 component (Martínez *et al.*,

2001b). Similar delayed attention effects localized to calcarine cortex have been observed in recordings of magnetic ERFs (Aine *et al.*, 1995; Noesselt *et al.*, 2002).

The present study aimed to provide a critical test of the hypothesis that enhanced long-latency neural activity elicited by attended-location stimuli actually arises from area V1 rather than from neighboring extrastriate areas. This test is based on the retinotopic organization of area V1, with the lower visual field projecting primarily to the upper bank of the calcarine fissure and the upper visual field primarily to the lower bank. In accordance with this anatomical arrangement, it is expected that stimuli presented to the upper and lower visual fields should elicit scalp potentials of opposite polarity for neural generators in primary cortex, as has been consistently observed for the C1/M1 components (Jeffreys and Axford, 1972; Clark *et al.*, 1995; Portin *et al.*, 1999; Di Russo *et al.*, 2001b). The present experiment investigated whether such a polarity inversion also occurs for long latency attention effects localized to calcarine cortex as subjects attend to stimuli presented in the upper or lower visual fields. Converging evidence on the localization of spatial attention effects in both striate and extrastriate areas was obtained by comparing sites of fMRI activation with the calculated positions of dipoles representing the attentional modulations

Materials and Methods

Subjects

Twenty-three volunteer subjects (13 female, mean age 23.2 years, range 18–35 years) gave written consent to participate in the main ERP experiment. A subset of 11 of these subjects (seven female, mean age 23.4 years, range 19–34 years) also received structural MRI scans. Seven of these subjects (four female, mean age 24.1 years, range 20–34 years) also received a separate session of task performance with fMRI scanning. All subjects were right-handed, as assessed by a brief questionnaire and had normal or corrected-to-normal visual acuity.

Stimuli

The standard stimuli (90% of total) consisted of sinusoidally modulated black and white checkerboards, circular in form, having a diameter of 2° of visual angle, a spatial frequency of four cycles per degree and a contrast of 50% (Fig. 1). Stimuli were presented in randomized sequences to one of four positions, one in each visual quadrant; the stimuli were centered along an arc that was equidistant (4°) from the fixation point and located at a polar angle of 25° above or 45° below the horizontal meridian. The stimuli were presented asymmetrically in this way so that the upper and lower field stimuli would activate approximately opposing sites on the lower and upper banks of the calcarine fissure, respectively, in light of evidence that the horizontal meridian is actually represented on the lower bank rather than in the lateral recess of the calcarine fissure (Clark *et al.*, 1995; Aine *et al.*, 1996).

The circular checkerboard stimuli were flashed for durations of 50 ms at a rapid presentation rate (SOAs varying between 250 and 550 ms). These stimuli were delivered on a gray field that was equal in luminance (60 cd/m^2) to the mean value of the sinusoidal checkerboard pattern. Each stimulus location was demarcated by four continuously present small dots placed at the corner of a box (2.2° square) within which the flashed circular stimuli were centered. Target stimuli consisted of similar circular checkerboards having a slightly smaller diameter (1.6–1.8°), which were presented to the same locations as the standards. Ten percent of the stimuli in each visual quadrant were targets, randomly intermixed with the standards.

Procedure

During the ERP recordings subjects were comfortably seated in a dimly lit, sound-attenuated and electrically shielded chamber while viewing stimuli presented on a 21-inch video monitor at a distance of 70 cm. Subjects were trained to maintain stable binocular fixation on a central dot (0.2°). The same stimuli and task were used in both the fMRI and ERP experiments except for the number of runs and the run durations. In the ERP experiment, the run durations were 100 s, each followed by a 30 s rest period, with occasional longer breaks interspersed. A total of 24 runs were carried out in order to deliver ~1300 standard stimuli to each quadrant. Subjects were instructed to direct their attention (without moving their eyes) to a particular quadrant according to four small arrows surrounding the fixation point that pointed to that quadrant. On a given run stimuli were presented only to either the upper or lower pair of quadrants, with the right/left order randomized. The task was to detect and respond to infrequent targets at the cued location with a button press while ignoring the stimuli in the opposite field. In the ERP experiment, the order of attention to the different quadrants was counterbalanced across runs. The responding hand was similarly counterbalanced across runs. Responses were classified as hits or false alarms according to whether or not they occurred within a 200–1200 ms window after the targets. ERPs to targets were not analyzed.

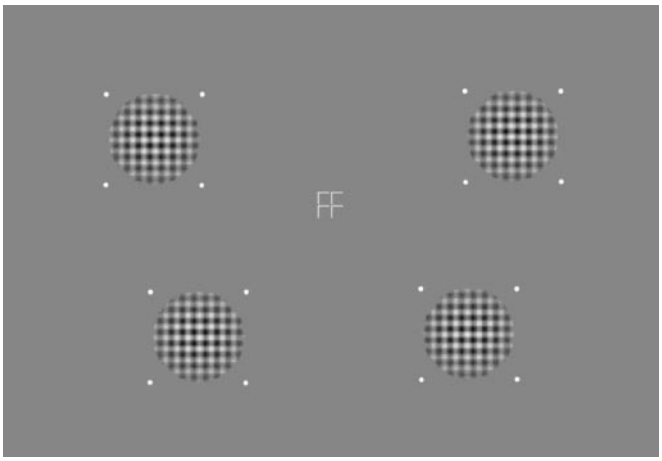

Figure 1. Standard stimuli used in this experiment. Small circular sinusoidal checkerboards were flashed in random order to right and left locations in either the upper or lower hemifields. Stimulus locations were continuously demarcated by four small dots.

The fMRI experiment consisted of eight runs of ~3 min each. Half of the runs presented upper quadrant stimuli and half lower quadrant stimuli. During each run the left and right quadrants were alternately cued for 20 s each.

The experiment began with a number of practice runs, in which the difficulty of the target discrimination was adjusted to achieve an average hit rate of 75–80% (number of targets correctly detected divided by the total number of targets occurring within the attended quadrant). The difficulty of the target discrimination was adjusted between runs if necessary to maintain this level of performance. The subjects received feedback on their behavioral performance and their ability to maintain fixation, as monitored by the electrooculogram (EOG).

Electrophysiological Recording and Data Analysis

The EEG was recorded from 64 electrodes using a modified 10–20 system montage. Standard 10–20 sites were FP1, FPz, FP2, F7, F3, Fz, F4, F8, T7, C3, Cz, C4, T8, P7, P3, Pz, P4, P8, O1, Oz, O2 and M1. Additional intermediate sites were, AF3, AFz, AF4, FC5, FC3, FC1, FCz, FC2, FC4, FC6, C5, C1, C2, C6, TP7, CP5, CP3, CP1, CPz, CP2, CP4, CP5, TP8, P5, P1, P2, P6, PO7, PO3, POz, PO4, PO8, I5, I3, Iz, I4, I6, SI3, SIz and SI4 [10–10 system (Nuwer *et al.*, 1998)]. All scalp channels were referenced to the right mastoid (M2). Horizontal eye movements were monitored with two bipolar electrodes at the left and right outer canthi (horizontal EOG). Vertical eye movements and blinks were recorded with an electrode below the left eye, which was also referenced to the right mastoid (vertical EOG).

The EEG from each electrode site was digitized at 250 Hz with an amplifier bandpass of 0.1–80 Hz (half amplitude low- and high-frequency cutoffs, respectively) with a 60 Hz notch filter and stored for off-line averaging. Computerized artifact rejection was performed prior to signal

averaging in order to discard epochs in which deviations in eye position, blinks, or amplifier blocking occurred. In addition, epochs that were preceded by a target stimulus within 1000 ms or followed within 500 ms were eliminated in order to avoid contamination by ERPs related to target detection and motor response. On average, 14% percent of the trials were rejected for violating artifact criteria.

Time-locked ERPs to standard (non-target) stimuli were averaged separately according to stimulus position (upper-left, upper-right, lower-right and lower-left) and whether that position was attended or unattended. To reduce high-frequency noise, the averaged ERPs were low-pass filtered at 46 Hz by convolving the waveforms with a gaussian function.

Repeated-measures analysis of variance (ANOVA) was used to evaluate attention effects on the different ERP components. The ANOVA factor was attention with respect to evoking stimulus (attended vs unattended). Separate ANOVAs were conducted on amplitudes and latencies for each ERP component of interest (i.e. C1, ipsilateral and contralateral P1, early N1, ipsilateral and contralateral late N1, and ipsilateral and contralateral P2). For these analyses, ERPs to left and right field stimuli were collapsed. Component amplitudes were measured as peak voltage deflections within specified time intervals (see Table 1) with respect to a 100 ms prestimulus baseline. These analyses were carried out at the electrode sites where the components were maximal in amplitude, separately for ERPs to upper and lower field stimuli (Table 1).

To compare the onset latencies of the C1 and the P1 attention effects, a further ANOVA was carried out on mean amplitude measures of these components at the sites where they were largest over successive 10 ms intervals with respect to the pre-stimulus baseline.

fMRI Scanning

Seven subjects were selected for participation in fMRI scanning on the basis of their ability to maintain steady visual fixation as assessed by EOG recordings during the ERP recording sessions. Stimuli were back-projected onto a screen inside the magnet bore and were viewed via a mirror situated directly above subjects' eyes.

Functional imaging was carried out on a Siemens VISION 1.5 T clinical scanner equipped with gradient echo-planar capabilities and a standard-equipment polarized surface coil optimized for brain imaging. Blood oxygen level dependent (BOLD) images were acquired with an echo planar imaging sequence (T_R = 2500 ms, T_E = 64 ms, flip angle = 90°) in the coronal plane (4 × 4 mm in-plane resolution). Seventy-four repetitions on each of 15 5 mm slices were acquired during each run; the first two repetitions were not used in the data analysis. Imaging began at the occipital pole and extended anteriorly.

For anatomical localization, high-resolution (1 × 1×1 mm) T_1-weighted images of the whole brain were acquired using a 3-D Magnetization Prepared Rapid Gradient Echo sequence (T_R = 11.4 ms, T_E = 4.4 ms, flip angle = 10°). Both anatomical and BOLD-weighted images were transformed into the standardized coordinate system of Talairach and Tournoux (Talairach and Tournoux, 1988).

Time-dependent echo-planar images were post-processed with AFNI software (Cox, 1996). Following three-dimensional motion correction, the raw time series data from each attend-upper and attend-lower field run were averaged within each individual. Group data were obtained by averaging the raw time series data over all subjects. Changes in signal strength related to the experimental manipulations were quantified by correlating the signal strength time series with a sequence of phase-shifted trapezoids representing the alternating conditions in the block design of the experiment (either attend-RVF versus attend-LVF). Linear drift was removed from the time series using Gram–Schmitt orthogonalization. Activations were considered significant for those voxels that correlated with the direction of attention with $r > 0.6$, $P < 0.005$ (uncorrected). To minimize the likelihood of falsely detecting spurious activations, only significantly correlated voxels occurring in clusters of four or more were considered in subsequent analyses. The probability that clusters of four or more voxels with correlations greater than 0.5 occurred by chance was estimated using Monte Carlo simulations to be 4% ($P = 0.04$).

Modeling of ERP Sources

Electrode positions were determined by means of a Polhemus spatial digitizer, which recorded the three-dimensional coordinates of each electrode and of three fiducial landmarks (the left and right preauricular points and the nasion). A computer algorithm calculated the best-fit sphere that encompassed the array of electrode sites and determined their spherical coordinates. The mean spherical coordinates for each site averaged across all subjects were used for the topographic mapping and source localization procedures. In addition, individual spherical coordinates were related to the corresponding digitized fiducial landmarks and co-registered with the landmarks identified on the whole-head MRIs of 11 subjects.

Spline interpolated topographical maps of scalp voltage were calculated (Perrin *et al.*, 1989) for ERPs to attended and unattended stimuli, and for the difference waves obtained by subtracting the unattended from the attended ERPs. Estimation of the dipolar sources of early ERP components in the grand-average waveforms was carried out using Brain Electrical Source Analysis [BESA version 2.1 (Scherg, 1990)]. In these calculations, BESA assumed an idealized three-shell spherical head model with the radius obtained from the average of the 23 subjects (87.2 mm), and the scalp and skull thickness of 6 and 7 mm, respectively.

A 'semi-seed model' approach for dipole source localization (Mangun *et al.*, 2001) was used in the present study. As starting positions, the dipole for each component was placed in the vicinity of the fMRI activation having Talairach coordinates closest to the location calculated for that component in a previous study (Di Russo *et al.*, 2001b). Then, single dipoles or dipole pairs were fit sequentially to the scalp voltage topographies over specific latency ranges (see Results) for each of the distinctive components in the waveform. These latency ranges were chosen to minimize overlap among the successive, topographically distinctive components. The ipsilateral dipole of each pair was constrained to be mirror image of the contralateral dipole in both location and orientation. The rationale behind this dipole fitting strategy was as follows: a single dipole was fit to the C1 component because the lateralized input pathways to the primary visual cortex predicts a unilateral source in that area. The subsequent P1 and N1 intervals were fit with bilateral mirror symmetric pairs of dipoles on the basis of the topographical maps obtained here and in previous studies (Mangun, 1995; Clark and Hillyard, 1996; Wijers *et al.*, 1997; Di Russo *et al.*, 2001) showing that the P1 and N1 have mirror image foci over the contralateral and ipsilateral occipital scalp, with the ipsilateral focus delayed by ~10–30 ms. Thus, the number of dipoles chosen for these models corresponded to the major topographical features of the ERP waveforms.

In a first analysis (model A), dipoles were fit simultaneously to both attended and unattended waveforms. In a second analysis (model B), dipoles were fit to the attend minus unattend difference waveforms after first including in the model the dipole that accounted for the C1 component in model A. Dipoles were fit sequentially in model B over the same time intervals as in model A. For comparison purposes, we carried out a further analysis identical to that of model A, with the only difference being that the dipoles were not seeded to the fMRI loci but started at an arbitrary positions (the center of the head).

In order to estimate the positions of the dipolar sources with respect to brain anatomy, the dipole coordinates calculated from the group average ERP distributions were projected onto the structural MRIs of individual subjects (Anllo-Vento *et al.*, 1998; Martínez *et al.*, 2001b; Di Russo *et al.*, 2001b), and the corresponding regions were identified on standard atlases (Damasio, 1995; Talairach and Tournoux, 1988). This allowed dipole positions to be expressed in Talairach coordinates.

Results

Behavioral Performance

The mean percent hits (75.3%) did not differ among stimulus positions [$F(3,66) > 1$; NS]. There was no effect of responding hand.

ERP Waveforms

Grand averaged ERPs in response to standard stimuli in each visual quadrant are shown in Figures 2 and 3. The ERP waveforms consisted of multiple spatially and temporally overlapping components. Peak amplitudes, latencies and effects

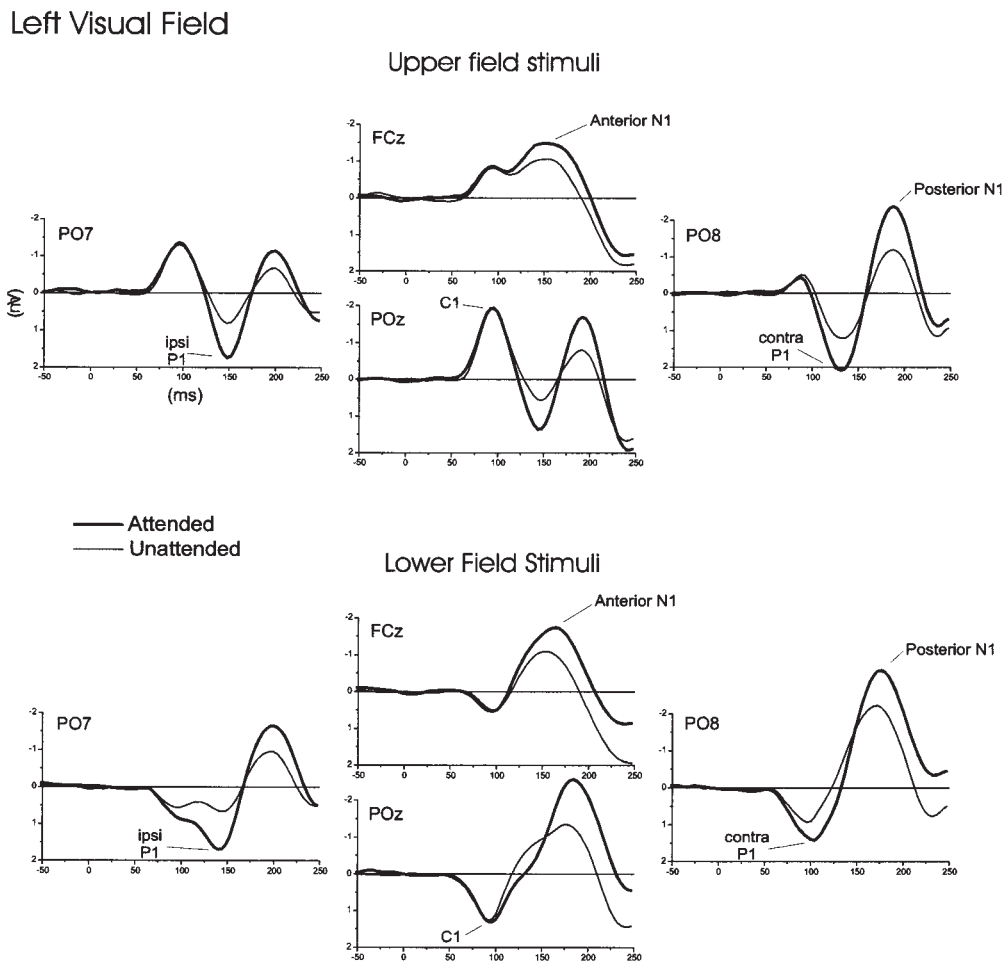

Figure 2. Grand average waveforms of the attended (thick line) and unattended (thin line) ERPs in response to the upper and lower left quadrant stimuli (standards).

of attention for each of these components are listed in Tables 1 and 2. At midline occipito-parietal sites, the ERP included a C1 component beginning at 50–60 ms and peaking at an overall mean latency of 93 ms with a negative polarity for the upper fields and positive polarity for the lower fields. In the ANOVA over successive 10 ms intervals the C1 (in both attended and unattended waveforms) became significantly different from baseline ($P < 0.05$) at 50–60 ms for the lower field stimuli and at 60–70 ms for the upper fields (at site POz). The P1 attention effect (measured in the attend minus unattend difference waves) became significant at 80–90 ms for lower field stimuli and at 90–100 ms for upper field stimuli at contralateral sites (PO3/PO4).

At lateral occipital sites the waveforms included a contralateral P1 peaking at a mean latency of 114 ms and an ipsilateral P1 at 140 ms. At fronto-central sites, the most prominent component was an early, anterior N1 with a mean latency of 148 ms. A late, posterior N1 component (178 ms contralateral, 195 ms ipsilateral) was prominent at occipito-parietal sites for the upper quadrants and at lateral occipital sites for the lower quadrants. Both contralateral (236 ms) and ipsilateral (248 ms) P2 components were largest at occipito parietal sites.

The earliest attention effect was on the contralateral P1, beginning at ~80–90 ms. Significant amplitudes increases were observed for both the contralateral and ipsilateral P1, as well as for all the N1 subcomponents. There were no significant effects of attention on the amplitudes of either the C1 or P2 components. No significant changes in latency were found as function of attention for any of the components (see Tables 2 and 3).

ERP Topography

The voltage topographic maps of C1, P1 and N1 components in the attended, unattended, and difference waveforms are shown in Figures 4 and 5 for the RVF stimuli. The corresponding maps for the LVF stimuli were virtually identical (but mirror image) and are not shown. For the upper quadrant stimuli, the C1 was maximally negative over midline parieto-occipital scalp regions, slightly ipsilateral to the visual field of the eliciting stimulus. For the lower quadrants, the C1 was maximally positive over midline parieto-occipital scalp regions, slightly contralateral to the visual field of the stimulus. For both upper and lower quadrants, the distribution of the P1 attention effect (attended minus unattended difference) was strongly contralateral in its early phase (70–100 ms), with an additional ipsilateral focus developing in its later phase (90–130 ms and 130–160 ms). The topographies of the early and late phases of the P1 attention effect also differed slightly, in that the late phase was more ventrally distributed and more widespread over both ipsilateral and contralateral occipital scalp areas. The early N1 attention effect (130–160 ms) had a maximal voltage over contralateral anterior scalp sites. The late N1 attention effect (170–190 ms) had a contralateral parieto-occipital focus that was situated more dorsally for lower field stimuli.

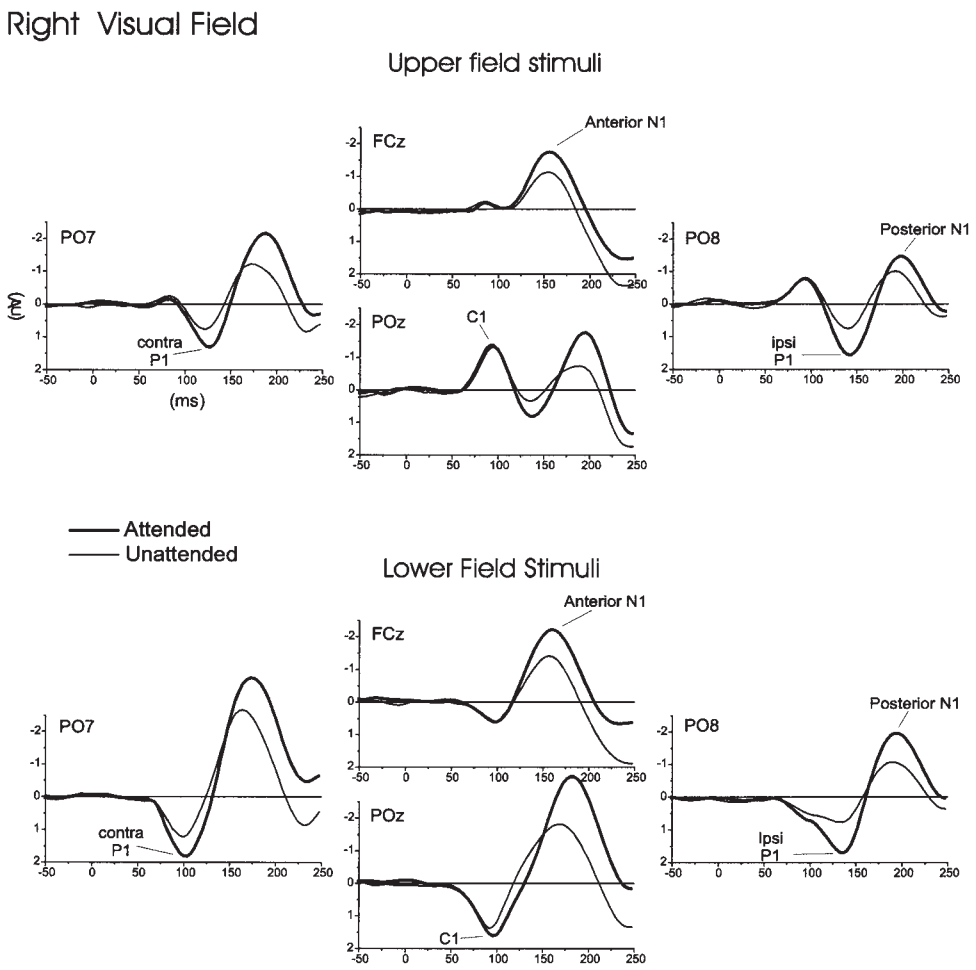

Figure 3. Grand average waveforms of the attended (thick line) and unattended (thin line) ERPs in response to the upper and lower right quadrant stimuli (standards).

fMRI Activations

Attention-related activations produced by the spatial attention task were greatest in the hemisphere contralateral to the attended visual field. It is likely that smaller ipsilateral fMRI activations were also present and corresponded to the neural activity that gave rise to the ipsilateral dipolar source activity. In the present fMRI analysis, however, which contrasted attend-left and attend-right conditions, such ipsilateral mirror foci would not be seen due to the dominance of the larger contralateral activations.

Following Di Russo and colleagues (Di Russo *et al.*, 2001b), the present analysis examines those activations that were located in proximity to the calculated positions of the dipoles that were fit to the C1, P1 and N1 distributions. These included activations in the calcarine fissure, the middle occipital gyrus and surrounding sulci, the fusiform gyrus, and the posterior parietal cortex. Figure 6 shows the significant attention-related hemodynamic changes in these regions (group average across all subjects), and Table 3 gives the Talairach coordinates of the centers of those activations.

Dipole Source Analysis

Using the BESA algorithm, dipoles were fit to both attended and unattended waveforms concurrently (model A) and, in a separate analysis, to the attend minus unattend difference waveforms (model B). Prior to fitting, the starting positions of the dipoles were placed at the fMRI-defined loci described below (see Table 3 for coordinates). Following the analysis of Di Russo and colleagues (Di Russo *et al.*, 2001b) dipoles were fit sequentially in the following order: first, a single dipole (no. 1) was placed on the calcarine activation and fit over 50–90 ms to account for the C1 component; second, the contralateral dipole in pair nos 2–3 was placed on the middle occipital activation, and the pair was fit over 72–104 ms to account for the early phase of the P1; third, the contralateral dipole in pair nos 4–5 was placed on the fusiform activation, and these were fit over 105–130 ms to account for the late phase of the P1; finally, the contralateral dipole in pair nos 6–7 was placed on the parietal activation, and the pair was fit over 135–165 ms to account for the anterior N1. The ipsilateral dipoles in pairs nos 2–3, nos 4–5 and nos 6–7 were constrained to be the mirror-image of the contralateral dipoles in both location and orientation. Aside from determining the starting points, the fMRI activations played no further role in the dipole fitting procedure.

Figures 7 and 8 show the calculated best-fit dipole positions for stimuli in each of the four quadrants for model A. The dipole positions for model B were very similar (compare Tables 4 and 5) and are not shown. [The unseeded model (with arbitrary dipole starting positions) yielded similar results: mean differences (averaged over all quadrants, in mm) between the positions of the dipoles in the seeded (model A) and the un-seeded model were as follows: C1 = 3.7, early P1 = 4.3, late P1 = 8.5, anterior

Table 1
Amplitudes (μV) and significance levels of attention effects on ERP components observed in this study

Component	Stimulus position	Electrode	Peak amplitude		$F(1,22)$	P
			Attended	Unattended		
C1 (70–100 ms)	upper	POz/POz	–1.62	–1.66	<1	NS
	lower	POz/POz	1.45	1.26	3.13	NS
P1 contra (90–130 ms)	upper	I5/I6	1.17	0.66	17.44	<0.0005
	lower	P7/P8	1.21	0.78	14.97	<0.001
P1 ipsi (130–160 ms)	upper	I5/I6	1.10	0.57	19.45	<0.0005
	lower	P7/P8	1.19	0.59	22.76	<0.0005
Anterior N1 (130–160 ms)	upper	FCz/FCz	–1.53	–0.99	27.94	<0.00001
	lower	FCz/FCz	–1.80	–1.18	29.89	<0.00001
Post. N1 contra (170–200 ms)	upper	PO3/PO4	–2.32	–1.24	34.91	<0.00001
	lower	P7/P8	–2.66	–1.86	31.32	<0.00001
Post. N1 ipsi (180–220 ms)	upper	PO3/PO4	–1.45	–0.78	16.87	<0.0005
	lower	P7/P8	–1.36	–0.72	15.53	<0.0007
P2 contra (200–260 ms)	upper	PO3/PO4	1.36	1.64	3.56	NS
	lower	PO3/PO4	1.28	1.40	2.21	NS
P2 ipsi (220–280 ms)	upper	PO3/PO4	0.88	0.90	<1	NS
	lower	PO3/PO4	0.66	0.78	1.65	NS

Base–peak measurements were made within the specified latency intervals (chosen to include the peaks in all subjects) at the first recording site for ERPs to right field stimuli and at the second recording site for left field stimuli. Amplitude values were averaged over ERPs to left and right field stimuli.

Table 2
Mean latencies (ms) and significance levels of attention effects of ERP components observed in this study

Component	Stimulus position	Electrode	Peak latency		$F(1,22)$	P
			Attended	Unattended		
C1	upper	POz/POz	94	95	<1	NS
	lower	POz/POz	92	92	<1	NS
P1 contra	upper	I5/I6	124	124	<1	NS
	lower	P7/P8	104	105	<1	NS
P1 ipsi	upper	I5/I6	142	146	<1	NS
	lower	P7/P8	136	138	<1	NS
Anterior N1	upper	FCz/FCz	148	147	<1	NS
	lower	FCz/FCz	148	148	<1	NS
Posterior N1 contra	upper	PO3/PO4	186	180	2.59	NS
	lower	P7/P8	174	172	<1	NS
Posterior N1 ipsi	upper	PO3/PO4	198	196	<1	NS
	lower	P7/P8	193	191	<1	NS
P2 contra	upper	PO3/PO4	240	238	<1	NS
	lower	PO3/PO4	232	234	<1	NS
P2 ipsi	upper	PO3/PO4	248	246	<1	NS
	lower	PO3/PO4	248	248	<1	NS

Measurements were made at first recording site for VEPs to right field stimuli and at second recording site for left field stimuli. Peak latency was calculated for average over left and right visual fields.

N1 = 7.5.] The time-varying source waveforms (also called dipole moments) are shown for model A at the left and model B at the right. As reported previously (Di Russo *et al.*, 2001b), a single dipole (no. 1) near the occipital midline accounted for the C1's voltage topography over the interval 50–90 ms. The earliest attention effect can be seen as an increased positivity in the source waveforms of the early contralateral P1 dipoles (no. 2 for LVF and no. 3 for RVF) starting at ~80 ms. A similarly increased positivity in the source waveforms of the late P1 dipoles (no. 4 and no. 5) began at 100–110 ms. These dipole pairs (nos 2–3 and nos 4–5) also accounted for the late posterior N1 components, which had scalp topographies very similar to those of the P1 (see Figs 4 and 5) over the time range 160–220 ms. The anterior N1 dipoles (nos 6–7) showed attentional modulation over the interval 120–180 ms. These models provided a very good fit to the observed ERP waveforms with low residual variance over both early and later time windows (Table 6).

The source waveform of the midline occipital dipole (no. 1) that was fit to the C1 component showed no evidence of attentional modulation over the 60–100 ms interval. However, starting at ~140 ms there was an increased amplitude in the attended source waveform that extended until ~220–230 ms. Importantly, this attention effect had the same polarity as the C1 peak for both upper and lower field stimuli. That is, like the C1 wave, the late attention effect inverted in polarity for upper versus lower field stimuli.

As noted above, the position of dipole no. 1 was determined by fitting the C1 during the early 50–90 ms interval, but its source waveform (together with those of the other dipoles) was generated throughout the entire epoch by the BESA algorithm. In BESA, the source waveforms are calculated by multiplying the inverse lead-field matrix of the dipoles by the recorded data waveforms (Scherg, 1990). This procedure decomposes the measured waveforms into separate contributions from the underlying source waveforms of each dipole in the model. The resulting source waveform for each dipole then represents the contribution of that source to the total surface-recorded voltage changes as a function of time. Accordingly, with the C1, P1 and

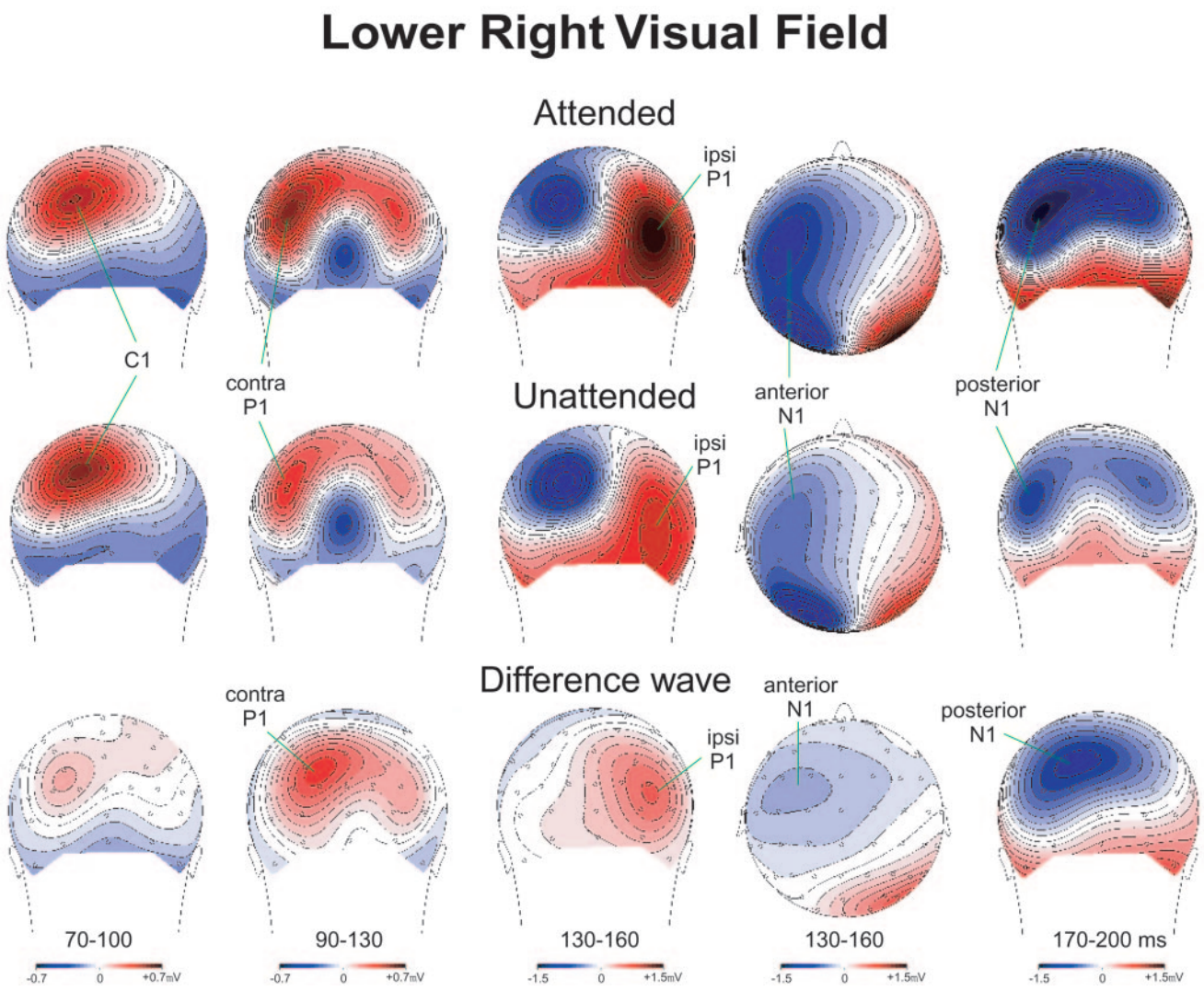

Figure 4. Spline-interpolated voltage maps derived from the grand averaged waveforms for ERPs to stimuli in the lower right quadrant. Maps are shown over successive time intervals for attended, unattended, and difference (attended minus unattended) waveforms.

anterior N1 dipoles having been fit over their respective time intervals, the longer-latency source waveforms of the C1 dipole represent its contribution to the recorded ERPs over that time range. This analysis shows that the same polarity-inverting dipolar sources that account for the early C1 could also account for the longer latency attention effect.

This late attention effect associated with the calcarine dipole could not be measured directly from the ERP waveforms, since it was overshadowed by the larger overlapping N1 modulations. Accordingly, its significance was tested in the grand average dipole source waveforms as follows: the attend minus unattend amplitude difference in the dipole source waveforms over successive 20 ms intervals (spanning 130–250 ms) was compared with respect to an estimate of the noise variability in this difference measure over the time window 0–68 ms, before any attention-related difference was evident. The late attention effect became significant in the 150–170 ms interval for the lower field stimuli and in the 170–190 ms interval for the upper field stimuli. The effect remained significant up to 230 ms for all quadrants but the lower left, which was significant until 250 ms (see Table 7).

Anatomical Localization

Figure 6 shows the anatomical positions of the dipolar sources in the difference wave model (model B, Table 5) superimposed upon averaged structural images and attention-related fMRI activations following co-registration of the BESA sphere with the MRI images. The mean C1 dipole position (dipole no. 1, from model A) was found to lie in the calcarine cortex for both the upper and lower field stimuli. The dipole pair accounting for the early P1 attention effect (dipoles nos 2–3) was found to lie in dorsal extrastriate cortex of the middle occipital gyrus, and the pair accounting for the late P1 effect (dipoles nos 4–5) was situated in the ventral fusiform gyrus. Dipole pair nos 6–7, which accounted for the early (anterior) N1 component, was localized in the parietal lobe near the intraparietal sulcus. Figure 6 shows a good correspondence between these calculated dipole positions and neighboring sites of fMRI activation, which can also be seen by comparing Tables 3 and 5.

Discussion

As in previous reports (see Introduction), the earliest effects of spatial attention on visual processing were manifest in the P1

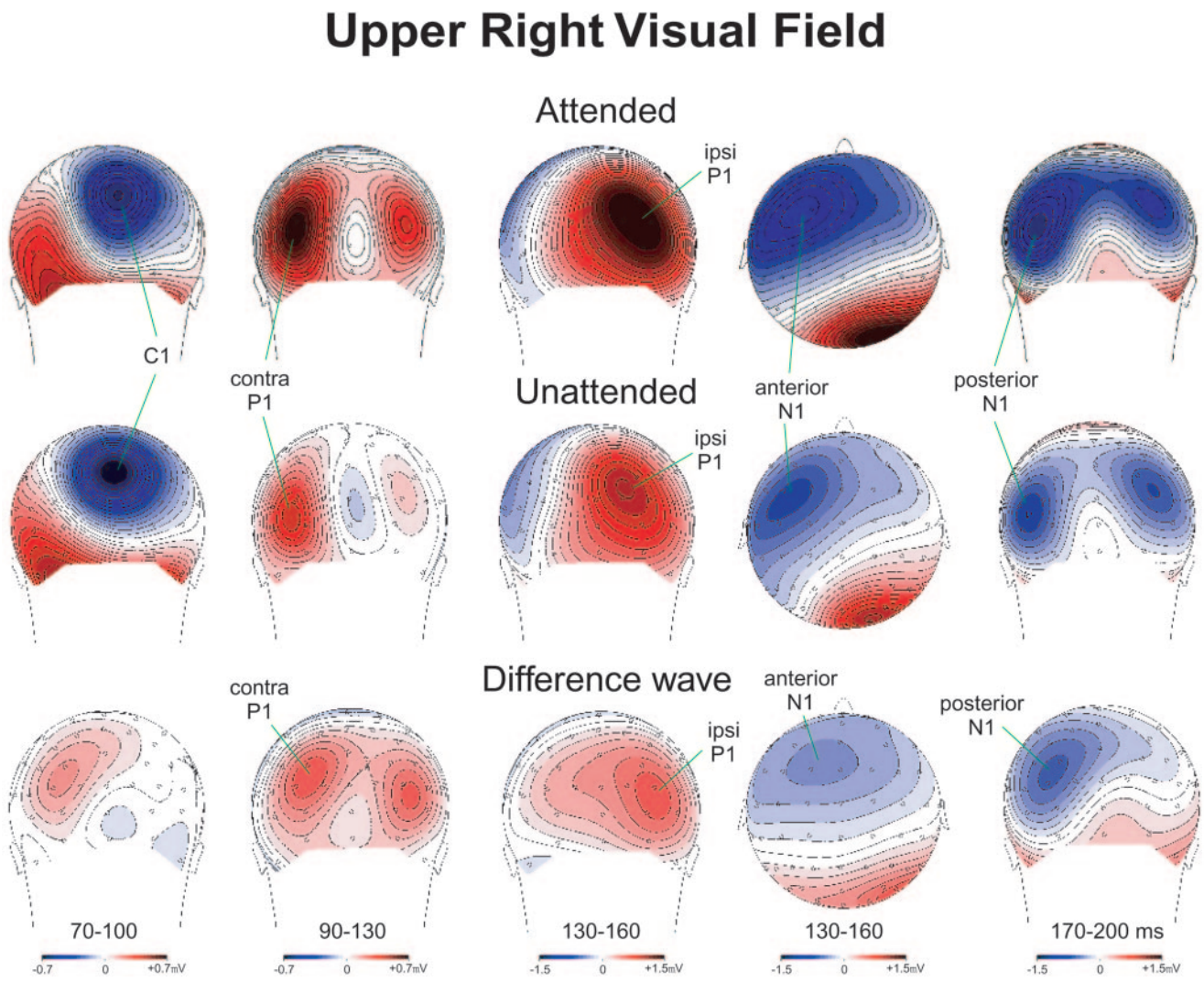

Figure 5. Same as Figure 4 for ERPs to stimuli in the upper right quadrant.

(onset 70–80 ms) and N1 (onset 130–150 ms) components, which were enlarged in amplitude in response to stimuli at attended locations in the visual field. Dipole modeling of these attention-related amplitude modulations and comparison of the calculated sources with fMRI activations indicated that they arose from multiple sites in extrastriate visual cortex. Also in accordance with previous reports, the initial C1 component (onset at 50–60 ms) was found to be unchanged by attention, and its calculated source location in calcarine cortex and polarity inversion for upper versus lower field stimuli were consistent with a neural generator in primary visual cortex (area V1). The major new finding was that the same dipole that was fit to the C1 component's distribution was also found to account for a longer latency attention effect (at 150–225 ms), which also inverted in polarity for upper versus lower field stimuli. This inversion, together with the co-localization of the C1/late effect dipole with attention-related fMRI activation in calcarine cortex, provides solid evidence that neural activity in area V1 is in fact modulated by attention but only after a delay, most likely mediated by feedback projections from higher extrastriate areas.

Several recent studies employing ERP and/or magnetic ERF recordings have also reported an enhanced neural response to attended-location stimuli that began at 130–150 ms and was localized to a dipolar source in calcarine cortex (Aine *et al.*, 1995; Martínez *et al.*, 2001b; Noesselt *et al.*, 2002). As in the present study, the calculated sources for the late activity were co-localized with or identical to the source that accounted for the initial C1/M1 component that was unaffected by attention. Moreover, in the studies of Martínez *et al.* (Martínez *et al.*, 2001b) and Noesselt *et al.* (Noesselt *et al.*, 2002) the dipoles accounting for the C1/M1 and the late attention effect were co-localized with attention-related fMRI activation in area V1 as defined by retinotopic mapping. Despite this converging evidence, however, the inverse dipole modeling approaches used may not be sufficiently accurate to distinguish between sources in immediately adjacent cortical areas such as V1 and V2. For this reason the present evidence of polarity inversion is critical for establishing a source in area V1. Such polarity inversion is consistent with the anatomical arrangement of the upper and lower field representations in area V1, which oppose each other across the calcarine fissure, but not with the organization of area V2, which is mainly situated on the mesial wall of the occipital lobe surrounding area V1 (Kaas, 1996; Wolf *et al.*, 1996; Kaas and Lyon, 2001). Thus, neural activity in both

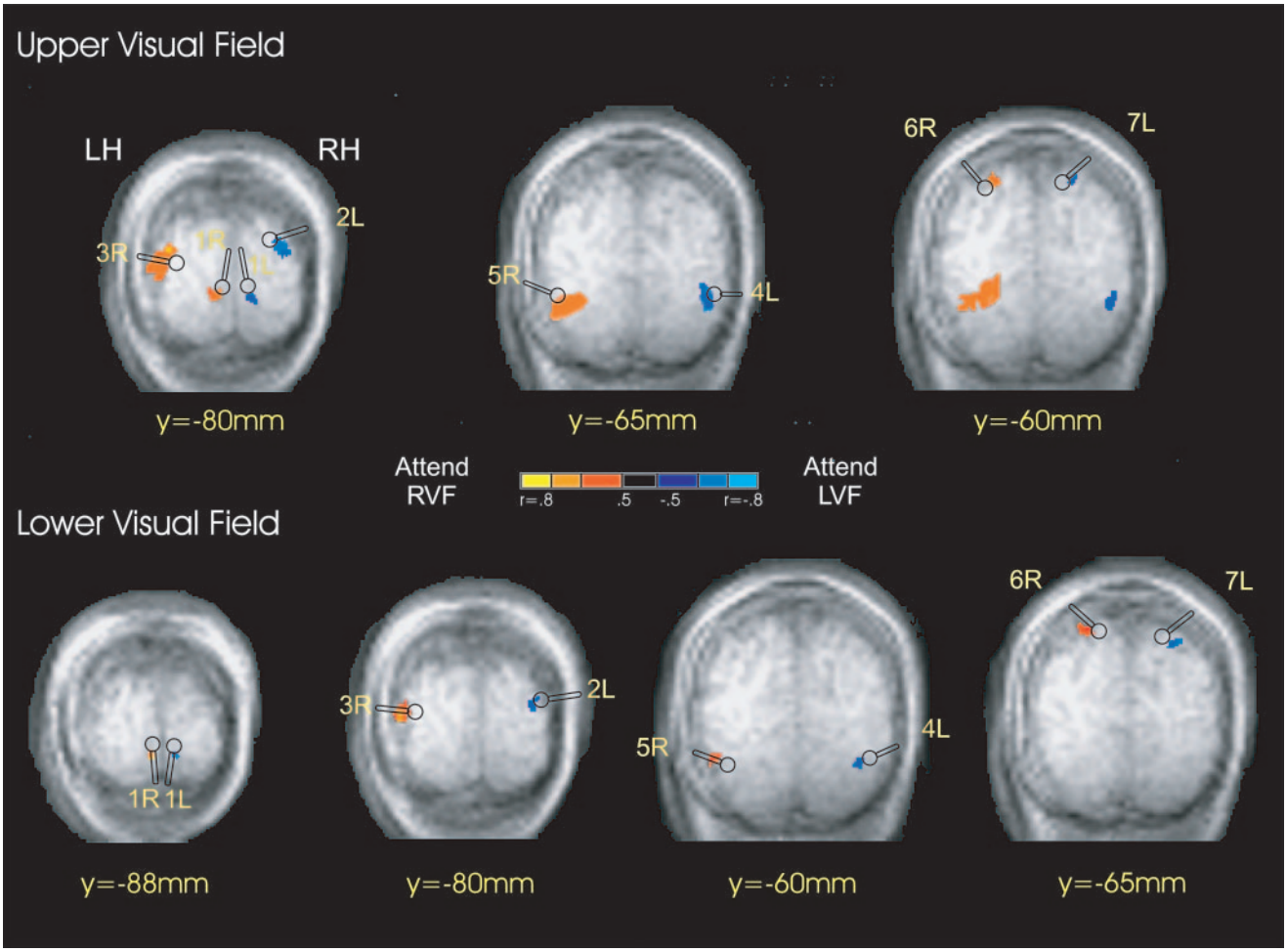

Figure 6. Spatial correspondence between attention-related fMRI activations (averaged across all seven subjects, Table 3) and the dipole models fit to the grand-average attentional difference waves (Table 5) for stimuli in the four quadrants. Red–orange spots represent greater activity during attend-RVF than attend-LVF. Blue spots represent greater activity during attend-LVF than attend-RVF. Millimeter values are Talairach *Y* coordinates of the slices that include the fMRI activations. Dipoles are projected onto those slices and hence may differ somewhat in their *y*-coordinates (compare Tables 3 and 5). Calcarine dipoles (dipole no. 1) obtained by fitting the attended and unattended waveforms concurrently (model A) are shown individually for RVF and LVF stimuli. For the paired dipoles, only the dipole contralateral to the visual field of the stimulus (designated R or L) is shown.

Table 3
Talairach coordinates of the significant contralateral striate, extrastriate and parietal activation sites averaged over seven subjects in the fMRI experiment (values are in mm)

	Stimulus position	Attend RVF > Attend LVF			Attend LVF > Attend RVF		
		X	*Y*	*Z*	*X*	*Y*	*Z*
Calcarine	upper	–11	–80	–7	10	–79	–8
	lower	–6	–87	–4	13	–86	–6
Dorsal	upper	–43	–72	8	40	–74	16
	lower	–40	–77	12	35	–77	14
Ventral	upper	–28	–65	–13	26	–61	–21
	lower	–42	–60	–18	41	–64	–16
Parietal	upper	–21	–61	45	28	–61	47
	lower	–27	–64	49	32	–55	40

Activations at these sites were positively correlated ($r > 0.6$) with attend-RVF and attend-LVF, respectively, at a significance level of $P < 0.005$.

the upper and lower visual field representations in area V2 would be expected to produce laterally oriented equivalent dipoles having the same left–right polarity. It is more difficult to predict how dipoles would be oriented in the more distant dorsal V3/ventral VP areas, but opposing vertically oriented sources seem very unlikely to arise from the complex geometry of these widely separated areas. Accordingly, it seems reasonable to conclude that the C1 and the late attention effect are both generated predominantly in area V1, although minor contributions from adjacent areas cannot be ruled out.

Recent studies in monkeys have sought to clarify the role of delayed feedback to area V1 in visual perception and attention. Single unit recordings from V1 have found that delayed neural activity is enhanced when a cell's receptive field falls on a figure/shape rather than on its background, suggesting a mechanism of figure/ground segregation (Lamme and Spekreijse, 2000; Lamme *et al.*, 2000; Lee and Nguyen, 2001). Such 'contextual influences' on V1 activity were hypothesized to depend upon feedback projections from higher visual areas where object recognition first takes place (Lamme and Spekreijse, 2000). This long latency contextual enhancement in V1 was found to be absent when the animal failed to detect the figure against the background, suggesting a relationship with conscious visual perception (Super *et al.*, 2001). In line with this suggestion, delayed activity in V1 was found to be augmented when attention was directed to a stimulus that fell on a cell's receptive field (Roelfsema *et al.*, 1998). Schroeder and colleagues (Schroeder *et al.*, 2001) have analyzed the synaptic mechanisms

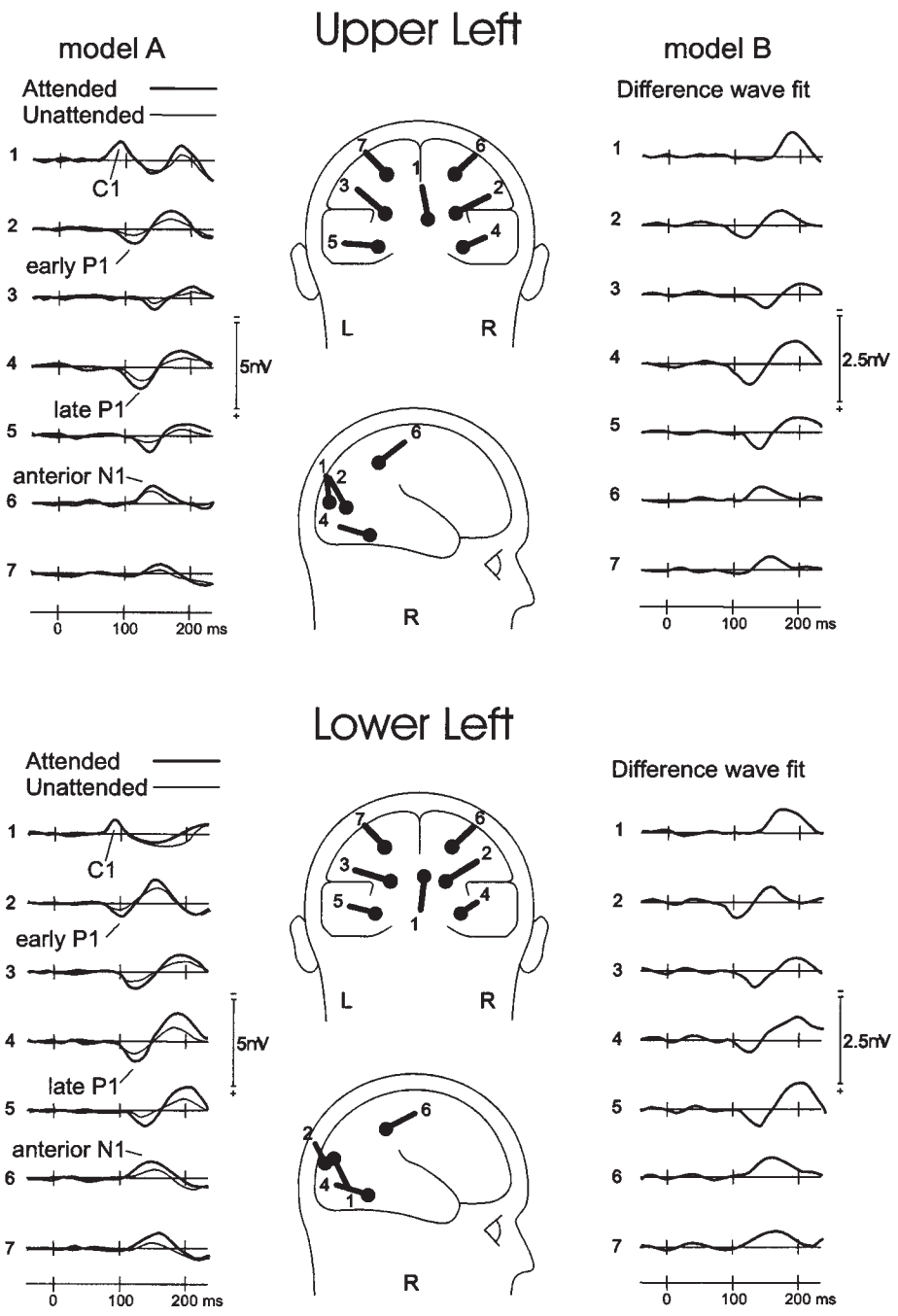

Figure 7. Dipole model of ERPs components elicited by standard stimuli located in the upper and lower left visual field. The left column shows time-varying source waveforms for each dipole in model A: thick lines are attended waveforms, thin are unattended. The middle column shows the location and orientation of the seven dipoles in model A. The right column shows time-varying source waveforms of the dipoles of model B, fit to the attended minus unattended difference waves.

involved in feedback projections to area V1 and proposed that they provide excitatory influences that enhance and prolong the neural representations of attended stimuli. Intracranial recordings of ERPs from human V1 have also shown delayed activity (at ~200 ms) that was modulated by contextual cuing of spatial information in a visual search task (Olson *et al.*, 2001). Together, these findings suggest that visual information is first enhanced by attention in higher extrastriate areas and is then conveyed to area V1 via reentrant feedback projections. This feedback may serve to improve the figure/ground segregation and the salience of objects within the spotlight of attention (Lamme and Spekreijse, 2000). It is also possible, however, that longer-latency interactions mediated by lateral connections within area V1 may contribute to delayed attention-related activity and contextual enhancement (Ito and Gilbert, 1999).

As in previous studies, the P1 (80–130 ms) and N1 (150–200 ms) were enlarged when attention was directed towards the location of the evoking stimuli (reviewed in Mangun *et al.*, 2001; Martínez *et al.*, 2001b). Both of these components had time-varying scalp distributions indicative of multiple neural sources. Dipole modeling showed that the early phase of the P1 enhancement (80–100 ms) could be accounted for by sources in

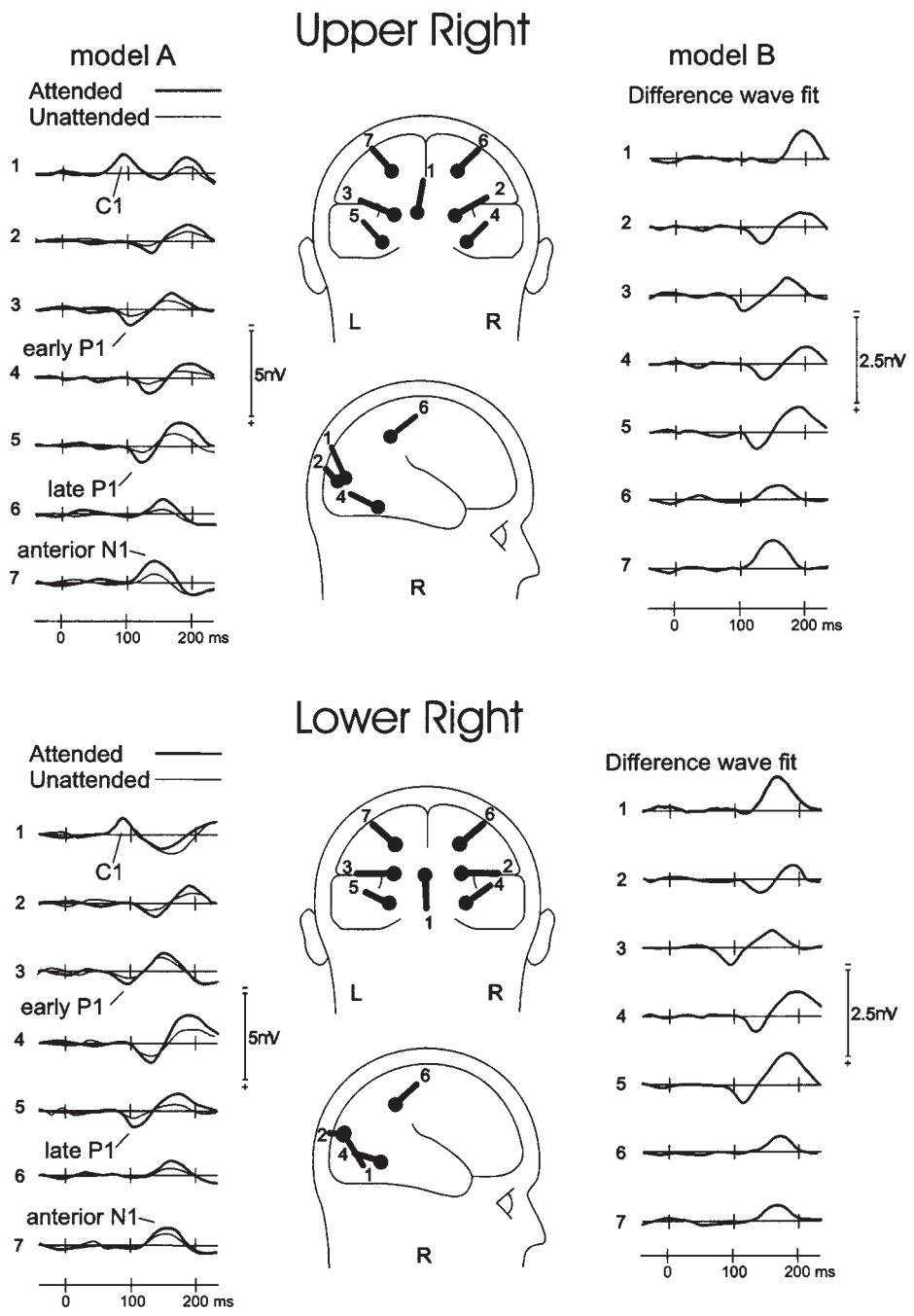

Figure 8. Same as Figure 7 for stimuli in the right visual field.

lateral mid-occipital cortex for both upper and lower field stimuli. These sources were in close proximity to attention-related fMRI activations in the middle occipital gyrus. The later phase of the P1 (100–130 ms) had a calculated dipolar source in ventral occipital cortex that was juxtaposed with a zone of fMRI activity in the posterior fusiform gyrus. This decomposition of the P1 wave into successive dorsal and ventral subcomponents is very similar to the analyses reported previously (Martínez *et al.*, 1999, 2001b; Di Russo *et al.*, 2001b). Although retinotopic mapping of the visual areas was not carried out in the present study, the Talairach coordinates of the P1 dipoles and the associated fMRI activations were in close proximity to those reported by Martínez and colleagues (Martínez *et al.*, 1999; 2001b) and by Di Russo *et al.* (Russo *et al.*, 2001b), who did carry out retinotopic mapping.

The spatial correspondence between the dipole positions and the foci of fMRI activation can only be regarded as suggestive, however. At present there is no generally accepted method for establishing with certainty that an ERP component and an fMRI signal change arise from the same neural activity pattern. Thus, we cannot rule out the possibility that neural activity associated with fMRI activity more distant from the dipoles than those reported here made a contribution to the surface-recorded ERPs.

Based on these comparisons, we propose that the early phase of the P1 attention effect corresponds to neural activity in areas V3/V3a and the region of the middle occipital gyrus immediately

Table 4
Average Talairach coordinates of dipoles in model A, fit to both the attended and unattended waveforms concurrently (values are in mm)

	Stimulus position	RVF			LVF		
		X	*Y*	*Z*	*X*	*Y*	*Z*
Calcarine (C1)	upper	–6	–82	–3	7	–71	–4
	lower	–3	–89	1	5	–85	–2
Dorsal occipital (early P1)	upper	±36	–80	10	±35	–82	14
	lower	±35	–78	18	±27	–90	18
Ventral occipito-temporal (late P1)	upper	±30	–57	–16	±30	–56	–20
	lower	±32	–58	–10	±31	–56	–13
Parietal (anterior N1)	upper	±24	–55	42	±24	–47	46
	lower	±24	–51	41	±24	–41	45

Table 5
Average Talairach coordinates of dipoles in model B, fit to the attended minus unattended difference waveforms

	Stimulus position	RVF			LVF		
		X	*Y*	*Z*	*X*	*Y*	*Z*
Dorsal occipital (early P1)	upper	±34	–80	11	±34	–82	13
	lower	±36	–79	15	±26	–90	18
Ventral occipito-temporal (late P1)	upper	±29	–56	–18	±29	–54	–19
	lower	±32	–55	–24	±31	–57	–14
Parietal (anterior N1)	upper	±25	–53	41	±25	–48	47
	lower	±23	–51	39	±26	–44	48

The calcarine dipole is omitted because it was derived from model A (values are in mm).

Table 6
Percentage of residual variance not accounted for by dipole models A and B in different time windows (expressed in ms)

Stimulus position	Model A		Model B	
	64–104	64–152	60–200	60–250
Upper left	1.96	1.32	1.15	1.76
Upper right	2.15	1.11	1.28	1.84
Lower right	2.46	2.12	1.88	2.33
Lower left	2.49	2.31	1.95	2.41

anterior to V3a, which has been termed area V7 (Hadjikhani *et al.*, 1998). In contrast, the later phase of the P1 enhancement appears to be generated in the ventral occipital region of area V4v and the immediately anterior region of the fusiform gyrus [termed V4 by McKeefry and Zeki (McKeefry and Zeki, 1997) and V8 by Hadjikhani and colleagues (Hadjikhani *et al.*, 1998)]. This suggests that the earliest spatial selection takes place in retinotopically organized extrastriate cortical areas, followed by enhanced processing of attended-location information in ventral stream areas specialized for pattern and object recognition (Martínez *et al.*, 2001b).

Like the P1, the subsequent N1 attention effect was found to arise from multiple extrastriate sources. The posterior N1 effect (170–200 ms) had a scalp distribution that overlapped with both the early and late phases of the P1 effect and was well accounted for by the sources fit to the P1. In contrast, the earlier, anterior phase of the N1 (130–160 ms) was modeled by a dipolar source in superior parietal cortex near fMRI activations in the vicinity of the intraparietal sulcus. This region of the parietal lobe is reportedly involved in tasks that require sustained covert attention to locations in the peripheral visual fields (Kastner *et al.*, 1999; Corbetta *et al.*, 2000; Hopfinger *et al.*, 2000; Sereno *et al.*, 2001). While this parietal area is generally considered to belong to the top-down control network for spatial attention (Nobre *et al.*, 1997; Corbetta, 1998), the present results suggest that visual input into the parietal lobe from attended sources is enhanced by spatial attention, which is in line with previous findings in monkeys (Colby and Goldberg, 1999).

A limitation of dipole modeling approaches such as that used here is their inability to determine whether the dipoles represent the activity of focal generator sources or the centroids of more distributed sources. Moreover, since the present analysis was based on grand average ERP waveforms, the calculated dipolar sources provide an estimate of neural activity patterns that were averaged across the anatomical variability of individual subjects. The validity of this approach is supported by the demonstration that inverse solution models of grand averaged waveforms yielded dipole parameters that were nearly identical to the mean values of the parameters of the individual subjects' dipolar sources (Clark *et al.*, 1995). It is difficult to estimate the accuracy of such dipole models, but the consistent localization of the C1 to the calcarine fissure and its proximity to fMRI activations in area V1 across several studies (Martínez *et al.*, 1999, 2001b; Di Russo *et al.*, 2001b; Noesselt *et al.*, 2002) suggest that the calculated dipole position has a margin of error of ~1.0–1.5 cm with respect to the centroid of V1 activity. It is more difficult to judge the accuracy of the P1/N1 dipole localizations, because the validity of a multi-dipole model depends on fitting the proper number of dipoles to correspond with the major sources of neural activity. In the present models, dipoles were fit to each of the observed major foci in the voltage topographic maps. The good correspondence between the calculated P1/N1 dipole positions and sites of fMRI activation suggests that this matching was approximately correct. The range of variability in P1/N1

Table 7
Significance levels of the attend minus unattend differences in the calcarine dipole source waveforms over successive 20 ms intervals spanning 130–250 ms

Time window	Upper left		Upper right		Lower left		Lower right	
	t	*P*	*t*	*P*	*t*	*P*	*t*	*P*
130–150	1.85	NS	1.51	NS	1.05	NS	< 1	NS
150–170	<1	NS	<1	NS	4.01	<0.001	3.82	<0.001
170–190	4.79	<0.0001	4.21	<0.0005	5.23	<0.0001	5.45	<0.0001
190–210	4.97	<0.0001	4.97	<0.0001	5.02	<0.0001	5.21	<0.0001
210–230	3.89	<0.001	5.32	<0.0001	4.88	<0.0001	5.12	<0.0001
230–250	1.78	NS	<1	NS	3.59	<0.002	<1	NS

Independent *t*-tests (df = 21) compared the attend minus unattend difference for five time points in each 20 ms interval with respect to 18 time points in the 0–68 ms baseline.

dipole localizations across the above-cited studies and the spatial coincidence of the dipoles with fMRI activations suggest a margin of positional error of ~2.0–2.5 cm with respect to the centroids of neural activity.

As in previous studies, the P1 and N1 attention effects took the form of amplitude increases without appreciable changes in waveforms or peak latencies. Moreover, the dipolar sources calculated for the P1 and N1 attention effects were very similar whether the dipoles were fit to the attend minus unattend difference waves or to the original attended and unattended waveforms. The dipoles accounting for these attention effects (and the associated fMRI activations) were also very similar in location to those that were fit to the P1 and N1 components evoked by the same stimuli under passive (non-attend) conditions in a previous study (Di Russo *et al.*, 2001b). Spatial attention experiments using fMRI have also reported a close correspondence between the visual-cortical areas activated by passive stimulation and those modulated by attention (Tootell *et al.*, 1998; Brefczynski and DeYoe, 1999; Martínez *et al.*, 2001b). These ERP and neuroimaging results provide strong support for the hypothesis that spatial attention acts to amplify sensory-evoked activity in the extrastriate cortex rather than recruiting additional populations of neurons (Hillyard and Muente, 1984; Posner and Dehaene, 1994; Hillyard *et al.*, 1998). This adds to the evidence from monkey neurophysiological studies indicating that spatial attention operates as a gain control mechanism that improves the effective signal strength of attended-location inputs (Reynolds *et al.*, 2000; Maunsell and McAdams, 2000).

In conclusion, the present ERP and fMRI data help to clarify the temporal sequence of stimulus selection processes in striate and extrastriate cortical areas. Strong support was given to previous proposals that visual inputs are not modified by spatial attention at the level of the initial geniculo-striate response in area V1 in the 50–90 ms range. Instead, the initial amplification of attended-location information was localized to retinotopically organized extrastriate areas in the interval 80–130 ms after stimulus onset. Evidence was obtained that these amplified signals are then routed forwards to higher visual areas of the occipito-temporal ventral stream and the parietal dorsal stream as well as backwards to the primary visual cortex in the time frame 130–225 ms. The polarity inversion of the late attention effect that was co-localized with fMRI activation in the calcarine cortex provided strong evidence for its generation in area V1. The source waveform of this late attention effect ascribed to area V1 bore a strong resemblance to the time course of single unit activity observed in monkey area V1 under the influence of contextual factors such as figure-ground relationships (Lamme and Spekreijse, 2000) and attention (Roelfsema *et al.*, 1998). This delayed, re-entrant input into V1 may enhance figure/ground segregation and improve the selection of relevant from irrelevant stimuli at attended locations in the visual field.

Notes

This work was supported by NIMH grant MH-25594. We thank Matt Marlow and Cecelia Kemper for technical assistance.

Address correspondence to Steven A. Hillyard, UCSD, Department of Neurosciences (0608), 9500 Gilman Drive, La Jolla CA, 92093-0608, USA. Email: shillyard@ucsd.edu URL: http://sdepl.ucsd.edu.

References

Aine CJ, Supek S, George JS (1995) Temporal dynamics of visual-evoked neuromagnetic sources: effects of stimulus parameters and selective attention. Int J Neurosci 80:79–104.

Aine CJ, Supek S, George JS, Ranken D, Lewine J, Sanders J, Best E, Tiee W, Flynn ER, Wood CC (1996) Retinotopic organization of human visual cortex: departures from the classical model. Cereb Cortex 6:354–361.

Anllo-Vento L, Luck SJ, Hillyard SA (1998) Spatio-temporal dynamics of attention to color: evidences from human electrophysiology. Hum Brain Mapp 6:216–238.

Brefczynski JA, DeYoe EA (1999) A physiological correlate of the 'spotlight' of visual attention. Nat Neurosci 2:370–374.

Clark V, Hillyard SA (1996) Spatial selective attention affects early extrastriate but not striate components of the visual evoked potential. J Cogn Neurosci 8:387–402.

Clark VP, Fan S, Hillyard SA (1995) Identification of early visually evoked potential generators by retinotopic and topographic analysis. Hum Brain Mapp 2:170–187.

Colby CL, Goldberg ME (1999) Space and attention in parietal cortex. Annu Rev Neurosci 22:319–349.

Corbetta M (1998) Frontoparietal cortical networks for directing attention and the eye to visual locations: identical, independent, or overlapping neural systems? Proc Natl Acad Sci 8:831–838.

Corbetta M, Kincade JM, Ollinger JM, McAvoy MP, Shulman GL (2000) Voluntary orienting is dissociated from target detection in human posterior parietal cortex. Nat Neurosci 3:292–297.

Cox RW (1996) AFNI — software for analysis and visualization of functional magnetic resonance neuroimages. Comput Biomed Res 29:162–173.

Damasio H (1995) Human brain anatomy in computerized images. New York: Oxford University Press.

Di Russo F, Spinelli D (1999a) Electrophysiological evidence for an early attentional mechanism in visual processing in humans. Vision Res 39:2975–2985.

Di Russo F, Spinelli D (1999b) Spatial attention has different effects on the magno- and parvo-cellular pathways. NeuroReport 10:2755–2762.

Di Russo F, Spinelli D, Morrone MC (2001a) Automatic gain control contrast mechanisms are modulated by attention in humans: evidence from visual evoked potentials. Vision Res 41:2335–2347.

Di Russo F, Martínez A, Sereno MI, Pitzalis S, Hillyard SA (2001b) The cortical sources of the early components of the visual evoked potential. Human Brain Mapping 15:95–111.

Eriksen CW, St. James JD (1986) Visual attention within and around the field of focal attention: a zoom lens model. Percept Psychophys 40:225–234.

Gandhi SP, Heeger D, Boynton GM (1999) Spatial attention affects brain

activity in human primary visual cortex. Proc Natl Acad Sci 96: 3314–3319.
Hadjikhani N, Liu AK, Dale AM, Cavanagh P, Tootell RB (1998) Retinotopy and color sensitivity in human visual cortical area V8. Nat Neurosci 1:235–241.
Heinze HJ, Mangun GR, Burchert W, Hinrichs H, Scholz M, Muente TF, Goes A, Scherg M, Johannes S, Hundeshagen H, Gazzaniga MS, Hillyard SA (1994) Combined spatial and temporal imaging of brain activity during visual selective attention in humans. Nature 372:543–546.
Hillyard SA, Muente TF (1984) Selective attention to color and locations: an analysis with event-related brain potentials. Percept Psychophys 36:185–198.
Hillyard SA, Vogel EK, Luck SJ (1998) Sensory gain control (amplification) as a mechanism of selective attention: electrophysiological and neuroimaging evidence. Philos Trans R Soc Lond B Biol Sci 353: 1257–1267.
Hopfinger JB, Buonocore MH, Mangun GR (2000) The neural mechanisms of top-down attentional control. Nat Neurosci 3:284–291.
Ito M, Gilbert, CD (1999) Attention modulates contextual influences in the primary visual cortex of alert monkeys. Neuron 22:593–604.
Jeffreys DA, Axford JG (1972) Source locations of pattern-specific component of human visual evoked potentials. I: Component of striate cortical origin. Exp Brain Res 16:1–21.
Kaas JH (1996) Theories of visual cortex organization in primates: areas of the third level. Prog Brain Res 112:213–221.
Kaas JH, Lyon DC (2001) Visual cortex organization in primates: theories of V3 and adjoining visual areas. Prog Brain Res 134:285–295.
Kastner S, Pinsk MA, DeWeerd P, Desimone R, Ungerleider LG (1999) Increased activity in human visual cortex during directed attention in the absence of visual stimulation. Neuron 22:751–761.
LaBerge D (1995) Computational and anatomical models of selective attention in object identification. In: The cognitive neurosciences (Gazzaniga MS, ed.), pp. 649–661. Cambridge, MA: MIT Press.
Lamme VAF, Spekreijse H (2000) Contextual modulation in primary visual cortex and scene perception. In: The new cognitive neurosciences (Gazzaniga MS, ed.), pp. 279–290. Cambridge, MA: MIT Press.
Lamme VA, Super H, Landman R, Roelfsema PR, Spekreijse H (2000) The role of primary visual cortex (V1) in visual awareness. Vision Res 40:1507–1521.
Lee TS, Nguyen M (2001) Dynamics of subjective contour formation in the early visual cortex. Proc Natl Acad Sci USA 98:1907–1911.
Luck SJ, Chelazzi L, Hillyard SA, Desimone R (1997) Neural mechanisms of spatial selective attention in areas V1, V2, and V4 of macaque visual cortex. J Neurophysiol, 77:24–42.
Mangun G R (1995) Neural mechanisms of visual selective attention. Psychophysiology, 32:4–18.
Mangun GR, Hinrichs H, Scholz M, Mueller-Gaertner HW, Herzog H, Krause BJ, Tellman, L, Kemna L, Heinze HJ (2001) Integrating electrophysiology and neuroimaging of spatial selective attention to simple isolated visual stimuli. Vision Res 41:1423–1435.
Martínez A, Anllo-Vento L, Sereno MI, Frank LR, Buxton RB, Dubowitz DJ, Wong EC, Hinrichs H, Heinze HJ, Hillyard SA (1999) Involvement of striate and extrastriate visual cortical areas in spatial attention. Nat Neurosci 2:364–369.
Martínez A, Di Russo F, Anllo-Vento L and Hillyard SA (2001a) Electrophysiological analysis of cortical mechanisms of selective attention to high and low spatial frequencies. Clin Neurophysiol 112:1980–1998.
Martínez A, Di Russo F, Annlo-Vento L, Sereno MI, Buxton R and Hillyard SA (2001b) Putting spatial attention on map: timing and localization of stimulus selection processes in striate and extrastriate visual areas. Vision Res 41:1437–1457.
Maunsell JHR, McAdams CJ (2000) Effects of attention on neuronal response properties in visual cerebral cortex. In: The new cognitive neurosciences (Gazzaniga MS, ed.), pp. 290–305. Cambridge, MA: MIT Press.
McKeefry DJ, Zeki S (1997) The position and topography of the human colour centre as revealed by functional magnetic resonance imaging. Brain 120:2229–2242.
Mehta AD, Ulbert I, Schroeder CE (2000a) Intermodal selective attention in monkeys I: distribution and timing of effects across visual areas. Cereb Cortex 10:343–358.
Mehta AD, Ulbert I, Schroeder CE (2000b) Intermodal selective attention in monkeys II: physiological mechanisms of modulation. Cereb Cortex 10:359–370.
Motter BC (1993. Focal attention produces spatially selective processing in visual cortical areas V1, V2 and V4 in the presence of competing stimuli. J Neurophysiol 70:909–919.
Nobre AC, Sebestyen GN, Gitelman DR, Mesulam MM, Frackowiak RS, Frith CD (1997) Functional localization of the system for visuospatial attention using positron emission tomography. Brain 120:515–533.
Noesselt T, Hillyard SA, Woldorff MG, Hagner T, Jaencke H, Tempelmann C, Hinrichs H, Heinze HJ (2002) Delayed striate cortical activation during spatial attention. Neuron 35:575–587.
Nuwer MR, Comi G, Emerson R, Fuglsang-Frederiksen A, Guerit JM, Hinrichs H, Ikeda A, Luccas FJ, Rappelsburger P (1998) IFCN standards for digital recording of clinical EEG. International Federation of Clinical Neurophysiology. Electroencephalogr Clin Neurophysiol 106:259–261.
Olson IR, Chun MM, Allison T (2001) Conextual guidance of attention: human intracranial event-related potential evidence for feedback modulation in anatomically early, temporally late stages of visual processing. Brain 124:1417–1425.
Perrin F, Pernier J, Bertrand O, Echallier JE (1989) Spherical splines for scalp potentials and current density mapping. Electroencephalogr Clin Neurophysiol 72:184–187.
Portin K, Vanni S, Virsu V, Hari R (1999) Stronger occipital cortical activation to lower than upper visual field stimuli. Exp Brain Res 124:287–294.
Posner MI, Dehaene S (1994) Attentional networks. Trend Neurosci, 17:75–79.
Posner MI, Snyder CR, Davidson BJ (1980) Attention and the detection of signals. J Exp Psychol 109:160–174.
Reynolds J, Desimone R (2001) Neural mechanisms of attentional selection. In: Visual attention and cortical circuits (Braun J, Koch C, Davis JL, eds), pp. 121–136. Cambridge, MA: MIT Press.
Reynolds JH, Pasternak T, Desimone R (2000) Attention increases sensitivity of V4 neurons. Neuron 26:703–714.
Ress D, Backus BT, Heeger DJ (2000) Activity in primary visual cortex predicts performance in a visual detection task. Nat Neurosci 3:940–945.
Roelfsema PR, Lamme VAF, Spekreijse H (1998) Object-based attention in the primary visual cortex of the macaque monkey. Nature 395: 376–381.
Scherg M (1990) Fundamentals of dipole source analysis. In: Auditory evoked magnetic fields and electric potentials (Grandori F, Hoke M, Roman GL, eds), pp. 40–69. Basel: Karger.
Schroeder CE, Mehta AD, Foxe JJ (2001) Determinants and mechanisms of attentional modulation of neural processing. Front Biosci 6: 672–684.
Sereno MI, Pitzalis S, Martínez A (2001) Mapping of contralateral space in retinotopic coordinates br a parietal cortical area in humans. Science 294:1350–1354.
Somers DC, Dale AM, Seiffert AE, Tootell RBH (1999) Functional MRI reveals spatially specific attentional modulation in human primary visual cortex. Proc Natl Acad Sci USA 96:1663–1668.
Super H, Spekreijse H, Lamme VA (2001) Two distinct modes of sensory processing observed in monkey primary visual cortex (V1). Nat Neurosci 4:304–310.
Talairach J, Tournoux P (1988) Co-planar stereotaxic atlas of the human brain. New York: Thieme.
Tootell RBH, Hadjikhani N, Hall EK, Marrett S, Vanduffel W, Vaughan JT, Dale AM (1998) The retinotopy of visual spatial attention. Neuron 21:1409–1422.
Vidyasagar TR (1998) Gating of neuronal responses in macaque primary visual cortex by an attentional spotlight. Neuroreport 9: 1947–1952.
Vidyasagar TR (1999) A neuronal model of attentional spotlight: parietal guiding the temporal. Brain Res Rev 30:66–76.
Wijers AA, Lange JJ, Mulder G, Mulder LJ (1997) An ERP study of visual spatial attention and letter target detection for isoluminant and non-isoluminant stimuli. Psychophysiology 34:553–565.
Woldorff MG, Fox PT, Matzke M, Lancaster JL, Veeraswamy S, Zamarripa F, Seabolt M, Glass T, Gao JH, Martin CC, Jerabek P (1997) Retinotopic organization of the early visual-spatial attention effects as revealed by PET and ERPs. Hum Brain Mapp 5:280–286.
Wolf F, Bauer HU, Pawelzik K, Geisel T (1996) Organization of the visual cortex. Nature 382(6589):306–307.
Wright RD (1998) Visual attention, vol. 8. Oxford: Oxford University Press.